

GROWTH OF GRAPHENE FILMS ON Pt(111) BY
THERMAL DECOMPOSITION OF PROPYLENE

THESIS

Presented to the Graduate Council of
Texas State University-San Marcos
in Partial Fulfillment
of the Requirements

for the Degree

Master of SCIENCE

by

Gregory S. Hodges, B.S.

San Marcos, Texas
May 2010

GROWTH OF GRAPHENE FILMS ON Pt(111) BY
THERMAL DECOMPOSITION OF PROPYLENE

Committee Members Approved:

Carl A. Ventrice, Jr., Chair

Wilhelmus J. Geerts

Nikoleta Theodoropoulou

Approved:

J. Michael Willoughby
Dean of the Graduate College

COPYRIGHT

by

Gregory S. Hodges

2010

ACKNOWLEDGEMENTS

I would like to thank my father for all the late night discussions of science and philosophy on the porch. And thanks to my mother for her consistent encouragement to pursue my interests.

I'd also like to present thanks to Dr Carl Ventrice Jr. Thank you for all your patience and guidance in the work of this thesis. I especially appreciate all the hands on training with machining, the guidance in setting up the UHV system and patiently answering my bombardment of ignoramus questions about experimental techniques. It is one thing to learn about physics in textbooks and lectures, and a completely other thing to build the equipment that enables observation.

This thesis was submitted on April 12, 2010.

TABLE OF CONTENTS

	Page
ACKNOWLEDGEMENTS	iv
LIST OF FIGURES	vii
ABSTRACT	ix
CHAPTER	
I. INTRODUCTION	1
A. WHAT IS GRAPHENE	1
B. GROWTH OF SINGLE LAYER GRAPHENE	2
II. CRYSTAL STRUCTURE	5
A. Pt(111) SURFACE	7
B. GRAPHENE	9
III. EXPERIMENTAL METHODS	12
A. ULTRA HIGH VACUUM	12
B. UHV CHAMBER DESIGN	16
C. SAMPLE HOLDER	20
D. LOW ENERGY ELECTRON DIFFRACTION	24
E. ELECTRON ENERGY LOSS SPECTROSCOPY	30
IV. EXPERIMENTAL RESULTS	34
A. CLEAN Pt(111) SURFACE	34
B. GRAPHENE GROWTH	37
i. Propylene deposition at room temperature followed by UHV annealing	37
ii. Propylene deposition at low temperature followed by UHV annealing	40
iii. Propylene deposition at high temperature followed by UHV annealing	42

V. DISCUSSION	46
VI. CONCLUSIONS	51
REFERENCES	53

LIST OF FIGURES

Figure	Page
2.1. Example of a non-Bravais crystal lattice	6
2.2. fcc crystal with the (111) plane highlighted	8
2.3. Schematic of (a) the real crystal lattice and (b) the reciprocal lattice of Pt	9
2.4. Crystal lattice of graphene	10
3.1. Ultra-high vacuum chamber	17
3.2. Copper sample holder in UHV	21
3.3. Schematic of copper sample holder	21
3.4. Schematic of the LEED optics	26
3.5. Schematic of (a) the vectors \mathbf{r}_1 and \mathbf{r}_2 from the two wave sources to a point of constructive interference and (b) the super-positioned wave crests	27
3.6. Schematic of electron energy loss spectroscopy	31
3.7. Picture of the EELS instrumentation	32
4.1. LEED of (a) high temperature anneal, no oxygen (b) post oxygen cleaning at 500 °C and (c) anneal at 500 °C, no oxygen	36
4.2. p(2x2) overlayer on a fcc(111) lattice	38
4.3. LEED of (a) clean (b) 1.6L dosing (c) 3.6L dosing at room temperature (E = 77.5 eV)	39
4.4. LEED of (a) 1.6L annealed at 500 °C (b) 3.6L annealed at 500 °C and (c) 3.6L annealed at 700 °C (E = 77.5 eV)	40
4.5. LEED of (a) clean (b) dosing 1.1L and (c) dosing 4.0L at -155°C (E = 77.5 eV)	41

4.6. LEED after (a) anneal at room temp and (b) anneal to 700 °C (E = 77.5 eV)	42
4.7. LEED of (a) clean (b) dosing 122L (c) annealed at 700 °C for 10min and (d) annealed at 700 °C for 20 min (E = 77.5 eV).....	43
4.8. LEED of (a) clean (b) dosing 6.1L and (c) annealed at 700 °C for 10 min (E = 77.5 eV)	44
4.9. LEED of (a) clean (b) dosing 0.97L (c) annealing at 700 °C for 10 min and (d) low temperature LEED at -165 °C (E = 77.5 eV)	45
5.1. Temperature dependent platinum-carbon solubility	47
5.2. LEED result of the Pt(111) crystal annealed to 1000 °C (E = 77.5 eV)	50

ABSTRACT

GROWTH OF GRAPHENE FILMS ON Pt(111) BY THERMAL DECOMPOSITION OF PROPYLENE

by

Gregory S. Hodges, B.S.

Texas State University-San Marcos

May 2010

SUPERVISING PROFESSOR: CARL A. VENTRICE JR.

Graphene is a single atomic layer of graphite. Several methods for producing graphene have been found, the first being the mechanical exfoliation from a graphite crystal. In this study we attempt to produce single-layer graphene by decomposition of propylene on the surface of Pt(111). Platinum has a face centered crystal structure, and the (111) plane forms a close-packed layer of atoms, which has a hexagonal symmetry. Graphene crystallizes in the honeycomb structure, which also has a hexagonal symmetry. Therefore, the Pt(111) surface has the proper symmetry for the growth of epitaxial graphene layers. Furthermore, platinum is a natural catalyst for the decomposition of organic molecules. The goal of this project was

to form graphene films by catalytic decomposition of propylene at a low enough temperature to prevent the solvation of carbon into the bulk of the platinum, which would cause multilayer graphene formation upon cooling of the crystal.

Two methods of growing graphene films were attempted: a) deposition of a propylene layer at low temperature (room temperature or at $-175\text{ }^{\circ}\text{C}$) followed by annealing and b) deposition of propylene on the platinum crystal that was held at high temperature ($475\text{ }^{\circ}\text{C}$). The deposition of propylene on Pt(111) at room temperature was found to form a $p(2\times 2)$ overlayer from the low energy electron diffraction measurements. Upon annealing, the $p(2\times 2)$ overlayer disappeared and a ring structure associated with graphene was found to form at $700\text{ }^{\circ}\text{C}$. Deposition of propylene at $-175\text{ }^{\circ}\text{C}$ resulted in an increase in diffuse background with no $p(2\times 2)$ diffraction pattern being observed. Annealing to $700\text{ }^{\circ}\text{C}$ also produced a ring structure associated with graphene. Dosing propylene at $475\text{ }^{\circ}\text{C}$ resulted in an almost total loss of the Pt(111) diffraction pattern for doses beyond a few Langmuir. Since carbon has a solubility of 0.5 atomic percent at $500\text{ }^{\circ}\text{C}$, the carbon atoms from the dissociated propylene are most likely diffusing into the surface region of the platinum. Because a temperature of $700\text{ }^{\circ}\text{C}$ is needed to order the graphene overlayer, it was determined that the relatively high solubility of carbon in platinum below $700\text{ }^{\circ}\text{C}$ prevents the formation of self-terminated single-layer graphene.

I. INTRODUCTION

A. WHAT IS GRAPHENE?

Graphene is an atomic monolayer of carbon that crystallizes in the honeycomb structure. In other words, it is a single layer of graphite. It is the two-dimensional analogue of the zero-dimensional buckyball and the one-dimensional carbon nanotube. There is a large interest within the scientific community in the growth and characterization of graphene since it has unique electrical, mechanical and thermal properties [1]. The unique electrical properties result from the true two-dimensional crystal structure. Because of these properties and its monolayer thickness, graphene shows promise for being used in the next generation of devices for the semiconductor industry.

The two-dimensional structure of graphene results in a linear energy band dispersion that allows electrons and holes to behave optically [2]. In other words, the carriers in graphene are predicted to behave as massless Dirac Fermions. Essentially, the electron transport is governed by Dirac's relativistic equation since the electrons move through the material at a significant fraction of the speed of light. This is due to the theoretical band structure of graphene being conic, linear in all directions, which causes the energy of the charge carriers to be directly proportional to their momentum instead of the usual classical result: the energy being proportional to the square of the momentum.

B. GROWTH OF SINGLE-LAYER GRAPHENE

One of the key issues associated with graphene is the development of techniques for the growth of large-area, single-layer films. Although carbon nanotubes have been used to make unique nanoscale devices, the precise placement and connection of millions of nanotube based devices to form an integrated circuit is a formidable challenge. If large area graphene films with lateral dimensions of a few cm^2 can be formed, photolithographic techniques can be used to simultaneously make millions of nanoscale devices.

There are several different approaches to growing and isolating single-layer graphene films. The original method developed by Geim [3] used micromechanical exfoliation from bulk graphite. In literal terms, a thin layer of graphite is peeled off a larger crystal of graphite, a thinner layer is then peeled off from that layer. The process is repeated until a single layer of graphene is produced. This mechanical exfoliation is a time consuming process that does not provide sheets of graphene large enough for most industrial applications.

Another promising method is epitaxial growth of graphene films under ultra-high vacuum (UHV) conditions. Epitaxy is a method of growing one crystalline material onto another. It is used in the semiconductor industry to make light emitting diodes, optical sensors, Schottky diodes, advanced integrated circuits and other devices in nanotechnology. Epitaxy is the most practical method for growing many nanoscale devices. There are two

basic approaches to growing epitaxial graphene films: vacuum evaporation of Si from SiC substrates [4] and growth on metal substrates by decomposition of a hydrocarbon source [5]. The main advantage of growing graphene on SiC is that the graphene film is formed directly on a semiconducting substrate ($E_g = 3.1$ eV for α -SiC), which is important for making graphene-based devices. However, graphene typically grows as a bilayer or multilayer on SiC, which can affect the true two-dimensional electronic properties, and the interaction of graphene with the optical phonons of the SiC substrate can adversely affect the electronic transport properties. In addition, the cost of device quality SiC substrates is prohibitively expensive (\$3k per 2" wafer).

The method that currently shows the most promise for producing large area single layer graphene is the catalytic decomposition of hydrocarbon sources on metal substrates. By using a metal surface that is catalytically active, the decomposition process will self-terminate at a single layer since exposure to the bare metal surface is needed for the decomposition of the hydrocarbon molecule. For this technique to work, the solubility of carbon in the metal substrate must be low at the growth temperature. Otherwise, carbon may precipitate from the bulk as the crystal is cooled, resulting in multilayer graphene formation. Once the single layer graphene is formed, it must be removed from the metal substrate since most applications require that the graphene be isolated on an insulating or semiconducting substrate. This is usually accomplished by etching the metal substrate away using an appropriate chemical etchant [6].

In this research project, we have studied the growth of graphene by the decomposition of

propylene on the Pt(111) surface. Platinum is catalytically active for the decomposition of many organic molecules, dissociating them under certain temperature and pressure regimes. Since graphene has a hexagonal symmetry, the Pt(111) surface was chosen since it also has a hexagonal symmetry. The primary method that was used for determination of the decomposition process was low energy electron diffraction (LEED). To perform these measurements, an UHV compatible sample holder was designed and constructed that allowed the transfer, sputtering, annealing, cooling, LEED measurements, and electron energy loss spectroscopy (EELS) measurements of the crystal.

II. CRYSTAL STRUCTURE

A crystal is defined to be a solid with its atoms arranged in an exact periodic order. A result of such periodic properties is that one crystal site is indistinguishable from any other similar site in the crystal. This is due to the fact that crystals have translational symmetry.

Crystals can have one, two or three dimensions. The most common, in reality, are three-dimensional crystals. A crystal is defined as a lattice plus a basis. The lattice is a mathematical construction that repeats throughout all space, whereas the basis defines the positions of the atoms in the crystal with respect to each lattice point. For crystals where each atom has an identical symmetry, one of the atoms can be chosen as a basis and then using the vector directions to the neighboring atoms, one can obtain the real-space position of any atom in the crystal

$$\mathbf{R} = n_1 \cdot \mathbf{x}_1 + n_2 \cdot \mathbf{x}_2 + n_3 \cdot \mathbf{x}_3 . \quad [2.1]$$

The vectors \mathbf{x}_1 , \mathbf{x}_2 and \mathbf{x}_3 are the real-space vectors separating individual atoms from their neighbors. The scalar values n_1 , n_2 and n_3 are used to obtain the real-space position, \mathbf{R} , of the atom located at the lattice point (n_1, n_2, n_3) .

The volume whose sides are the basis vectors \mathbf{x}_1 , \mathbf{x}_2 and \mathbf{x}_3 is called a unit cell of the lattice, in that, if such a cell is translated by all the lattice vectors, the volume of the

whole lattice is covered once and only once [7]. The primitive cell is the smallest volume that produces such coverage. The volume of the unit cell is given by $\Omega_c = \mathbf{x}_1 \cdot (\mathbf{x}_2 \times \mathbf{x}_3)$.

A crystal lattice can either be Bravais or non-Bravais. In a Bravais-lattice, all lattice points are equivalent, and hence by necessity all atoms in the crystal are of the same kind [7]. The non-Bravais lattice does not have this equivalency among all lattice points. An example of a non-Bravais lattice is illustrated below. Clearly the points A', B', C' and D' are equivalent to each other and so are A, B, C and D. However, the points A and A' are not equivalent. This crystal is said to have a basis.

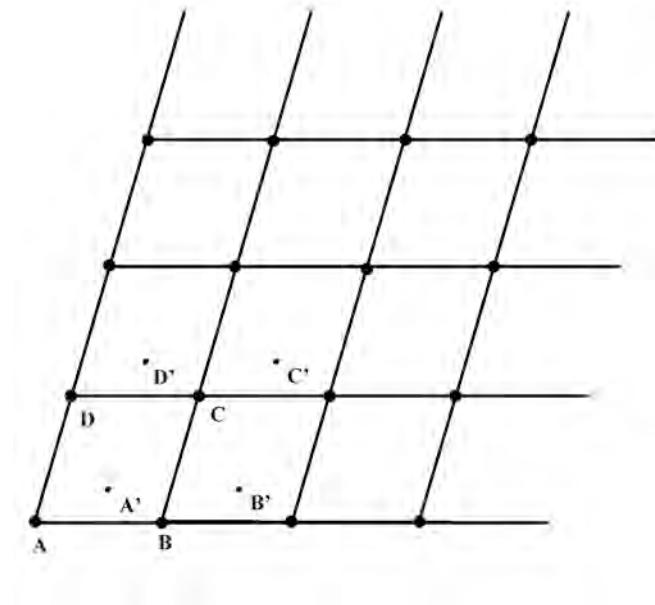


Figure 2.1. Example of a non-Bravais crystal lattice.

In 3-dimensions, there are only 14 Bravais crystal lattices and 230 non-Bravais lattices [7]. The 14 Bravais lattices can be broken into 7 groups, known as crystal systems.

These crystal systems are called Triclinic, Monoclinic, Orthorhombic, Tetragonal, Cubic, Trigonal and Hexagonal.

Each crystal lattice also has its reciprocal lattice structure. This structure can be constructed from the basis vectors of the original lattice. Using \mathbf{x}_1 , \mathbf{x}_2 and \mathbf{x}_3 as our basis vectors, the reciprocal lattice vectors \mathbf{x}_1^* , \mathbf{x}_2^* , and \mathbf{x}_3^* are defined by

$$\mathbf{x}_1^* = \frac{2\pi}{\Omega_c} (\mathbf{x}_2 \times \mathbf{x}_3) , \quad [2.2]$$

$$\mathbf{x}_2^* = \frac{2\pi}{\Omega_c} (\mathbf{x}_3 \times \mathbf{x}_1) , \quad [2.3]$$

$$\mathbf{x}_3^* = \frac{2\pi}{\Omega_c} (\mathbf{x}_1 \times \mathbf{x}_2) , \quad [2.4]$$

where Ω_c is the volume of a unit cell [7]. These new vectors now form the basis of our reciprocal lattice by

$$\mathbf{G} = n_1 \mathbf{x}_1^* + n_2 \mathbf{x}_2^* + n_3 \mathbf{x}_3^* . \quad [2.5]$$

A. Pt(111) SURFACE

Platinum crystallizes in the face centered-cubic (fcc) crystal structure. This structure is defined by having an atom at each corner of a cube, along with an atom at the center of each face of the cube. Cutting along the (111) plane of the crystal creates a hexagonal array of close packed atoms.

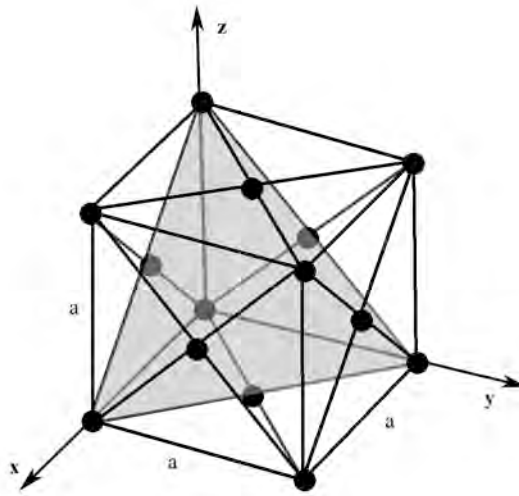


Figure 2.2. fcc crystal with the (111) plane highlighted.

Treating each atom in the crystal as a lattice point, the atomic distance between each atom in the (111) plane is $d = a/\sqrt{2}$, where a is the length of the side of the conventional cubic cell. For platinum, the lattice constant is $a = 3.92 \text{ \AA}$ and the nearest neighbor distance between atoms is $d = 2.77 \text{ \AA}$. This gives the following vector basis for the conventional cubic cell,

$$\mathbf{R} = a\mathbf{i} + a\mathbf{j} + a\mathbf{k} . \quad [2.6]$$

Using these, the basis vectors for the (111) plane of the fcc lattice can be defined as

$$\mathbf{R}_{(111)} = d\mathbf{i}' + d\mathbf{j}' , \quad [2.7]$$

where \mathbf{i}' and \mathbf{j}' are defined as

$$\mathbf{i}' = \frac{1}{\sqrt{2}}\mathbf{i} - \frac{1}{\sqrt{2}}\mathbf{k} \text{ and} \quad [2.8]$$

$$\mathbf{j}' = \frac{1}{\sqrt{2}}\mathbf{j} - \frac{1}{\sqrt{2}}\mathbf{k} . \quad [2.9]$$

The unit vectors in the local surface space of the (111) lattice are

$$\mathbf{x}_1 = \langle 1, 0 \rangle \text{ and} \quad [2.10]$$

$$\mathbf{x}_2 = \left\langle \frac{1}{2}, \frac{\sqrt{3}}{2} \right\rangle. \quad [2.11]$$

Using the equations for the reciprocal lattice vectors the following results for the reciprocal surface lattice

$$\mathbf{x}_1^* = \frac{4\pi}{\sqrt{3}} \left\langle \frac{\sqrt{3}}{2}, -\frac{1}{2} \right\rangle \text{ and} \quad [2.12]$$

$$\mathbf{x}_2^* = \frac{4\pi}{\sqrt{3}} \langle 0, -1 \rangle. \quad [2.13]$$

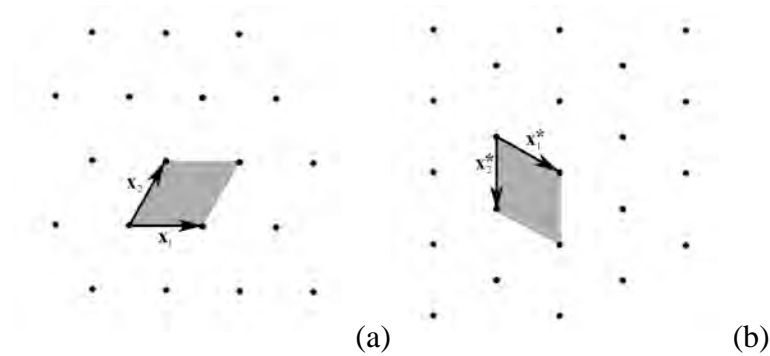


Figure 2.3. Schematic of (a) the real crystal lattice and (b) the reciprocal lattice of Pt.

B. GRAPHENE

Graphene is a single layer of sp^2 bonded carbon atoms that form a two-dimensional honeycomb crystal. In other words, it is a single atomic layer of graphite. Graphite can crystallize in one of two different forms: the α -phase, which has an ABAB stacking sequence, and the β -phase, which has an ABCABC stacking sequence. The α -phase can be converted to the β -phase through mechanical treatment and the β -phase converts to the α -phase at higher temperatures.

The structure of graphene can be thought of as a series of tiled hexagons, as can be seen in the image below.

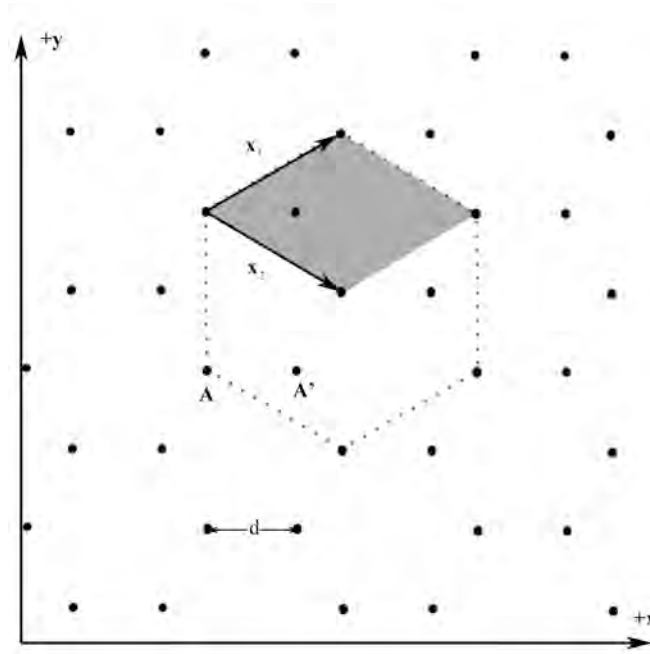


Figure 2.4. Crystal lattice of graphene.

This is a 2-dimensional crystal, but it is not a Bravais lattice. The Bravais lattice requires that each point in the lattice is equivalent (i.e. translating from one point to another is indistinguishable from another). As we can see, translating from point A to A' , the sites are not equivalent. The crystal looks different from someone standing on A and looking in the $+x$ -direction as opposed to someone standing on A' and looking in the $+x$ -direction.

Since the crystal is non-Bravais, it has a basis. In case of graphene, the lattice is hexagonal and the basis has two atoms. Therefore, the length of the basis vectors of the

lattice is longer than the distance between two adjacent carbon atoms. The following are the basis vectors for graphene

$$\mathbf{x}_1 = \frac{a}{\sqrt{2}}\mathbf{i} - \frac{a}{\sqrt{2}}\mathbf{j} \text{ and} \quad [2.14]$$

$$\mathbf{x}_2 = \frac{a}{\sqrt{2}}\mathbf{i} + \frac{a}{\sqrt{2}}\mathbf{j} . \quad [2.15]$$

The lattice constant of graphene is $a = 2.46 \text{ \AA}$, and the nearest neighbor distance of the carbon atoms is $d = a/\sqrt{3} = 1.42 \text{ \AA}$. The honeycomb structure can be thought of as two Bravais lattices that are superimposed onto each other. As can be seen from a comparison of the close-packed layer of atoms of the Pt(111) surface and the honeycomb structure of graphene, they both have hexagonal symmetry. This similarity should make Pt(111) a natural fit for growing well-ordered graphene on the surface. However, we can see that there is a lattice mismatch due to the difference in lengths of the basis vectors of the Pt(111) surface and graphene. This results in a mismatch of approximately 11%. Ideally, it would be best to grow on a surface with a mismatch of 0%.

Similarly for the Pt(111) crystal the reciprocal lattice of graphene is calculated to be

$$\mathbf{x}_1^* = \sqrt{2}\pi a\mathbf{i} - \sqrt{2}\pi a\mathbf{j} \text{ and} \quad [2.16]$$

$$\mathbf{x}_2^* = -\sqrt{2}\pi a\mathbf{i} + \sqrt{2}\pi a\mathbf{j} . \quad [2.17]$$

III. EXPERIMENTAL METHODS

A. ULTRA-HIGH VACUUM

Ultra-high vacuum is classified as a pressure of 10^{-9} Torr or lower. Under such conditions the mean free path of a molecule is much larger than the typical dimensions of a vacuum chamber. This means that a free gas particle will interact with the walls of the chamber many times before colliding with another free molecule. An indirect result of this is that most reactions occur on the surfaces of materials in the chamber.

The mean free path of a molecule can be derived from the kinetic theory of gases.

Assuming a spherical molecule diameter d , then the cross sectional area of two colliding particles is πd^2 and if a particle collides with another particle in time t at an average relative velocity $\sqrt{2}v$ then the volume of collision is given by

$$V = \pi d^2 \sqrt{2}vt . \quad [3.1]$$

The square root of two is required due to the result of the average relative velocity of one particle with another particle. Between any two particles with velocities \vec{v}_1, \vec{v}_2 that have magnitudes of the average particle velocity then the relative velocity is given by

$$\bar{v}_{rel} = \bar{v}_1 - \bar{v}_2 . \quad [3.2]$$

This relation can be used to derive the magnitude of the average relative velocity by using the dot product.

$$\begin{aligned} |\bar{v}_{rel}| &= \sqrt{\bar{v}_{rel} \cdot \bar{v}_{rel}} \\ &= \sqrt{\bar{v}_1 \cdot \bar{v}_1 - 2\bar{v}_1 \cdot \bar{v}_2 + \bar{v}_2 \cdot \bar{v}_2} \\ &= \sqrt{v^2 + v^2} \\ &= \sqrt{2}v \end{aligned} \quad [3.3]$$

The dot product between \bar{v}_1 and \bar{v}_2 averages to zero since the dot product between the two vectors involves the cosine of the angle between them; integrating over all possible angles evaluates to zero.

Because the volume of collision only contains a single molecule we can equate it the inverse of n_v , number of molecules per unit volume.

$$\pi d^2 \sqrt{2}vt = \frac{1}{n_v} . \quad [3.4]$$

Multiplying the right hand side of the equation by $\frac{vt}{l}$, the distance traveled divided by the mean free path, and solving for the mean free path yields

$$l = \frac{1}{n_v \sqrt{2\pi} d^2} . \quad [3.5]$$

Using the ideal gas law we can solve for the number of molecules per unit volume in terms of pressure P , temperature T and the Boltzmann constant k_B . This results in the following equation for the mean free path of a molecule

$$l = \frac{k_B T}{P \sqrt{2\pi} d^2} . \quad [3.6]$$

Under UHV conditions the gas is sufficiently dilute that the motion of the gas molecules is well described by kinetic theory. The flux of a dilute gas impinging on a surface is given by

$$\Phi_0 = \frac{P}{\sqrt{2\pi m k_B T}} = 3.5 \times 10^{22} \frac{P}{\sqrt{MT}} \text{ (cm}^{-2}\cdot\text{s}^{-1}\text{)}, \quad [3.7]$$

where P is the gas pressure in Torr, m is the mass of the molecule in kg, M is the molecular weight of the molecule in g/mol, k_B is the Boltzmann constant, and T is the absolute temperature in K. Therefore, the time to form a full monolayer of adsorbed gas molecules on a surface is given by

$$t_{ML} = \frac{\eta_a}{\Phi_0 S N_d} = 2.9 \times 10^{-23} \frac{\eta_a \sqrt{MT}}{S N_d P} , \quad [3.8]$$

where η_a is the number of adsorption sites per cm^2 on the surface, S is the sticking coefficient of the adsorbing gas molecule, and N_d is the dissociation coefficient. For instance, if molecular oxygen dissociates into atomic oxygen upon adsorption, the dissociation coefficient would be $N_d = 2$. The sticking coefficient depends both on the reactivity of the surface and the temperature. For very reactive surfaces or at low temperatures, the sticking coefficient approaches $S = 1$. The (111) surface of a face-centered cubic (fcc) crystal forms a close packed array of atoms. Therefore, the number of atoms per area for the fcc(111) surface is given by

$$\eta = \frac{4}{\sqrt{3}a_0^2}, \quad [3.9]$$

where a_0 is the lattice constant of the crystal. For Pt(111) which is a fcc crystal, this results in $\eta = 1.5 \times 10^{15} \text{ cm}^{-2}$ since $a_0 = 3.92 \text{ \AA}$. If molecular oxygen is dosed on the Pt(111) surface, it forms a p(2x2) overlayer of oxygen atoms (*i.e.*, $\eta_a = \eta/4$). For dosing molecular oxygen at a pressure of $P = 1 \times 10^{-6} \text{ Torr}$ at $T = 25 \text{ }^\circ\text{C}$, a monolayer of atomic oxygen will form in approximately 0.5 s. However, under typical UHV conditions of $P = 1 \times 10^{-10} \text{ Torr}$, it will typically take several hours to form a monolayer of contaminants on a surface. When gas molecules are dosed on surfaces, the unit of dosage is defined as a Langmuir (L), where

$$1 \text{ L} = 1 \times 10^{-6} \text{ Torr}\cdot\text{s} . \quad [3.10]$$

B. UHV CHAMBER DESIGN

Our system is a stainless steel vacuum chamber with a variety of pumps attached, which allows us to obtain UHV. The chamber is grounded, which results in a electric field free region inside the chamber for doing LEED and EELS. The chamber also has a load lock for insertion of samples into the chamber without breaking UHV. The pumps used on our system include two rotary vane pumps, two turbo pumps, a titanium sublimation pump and two ion pumps.

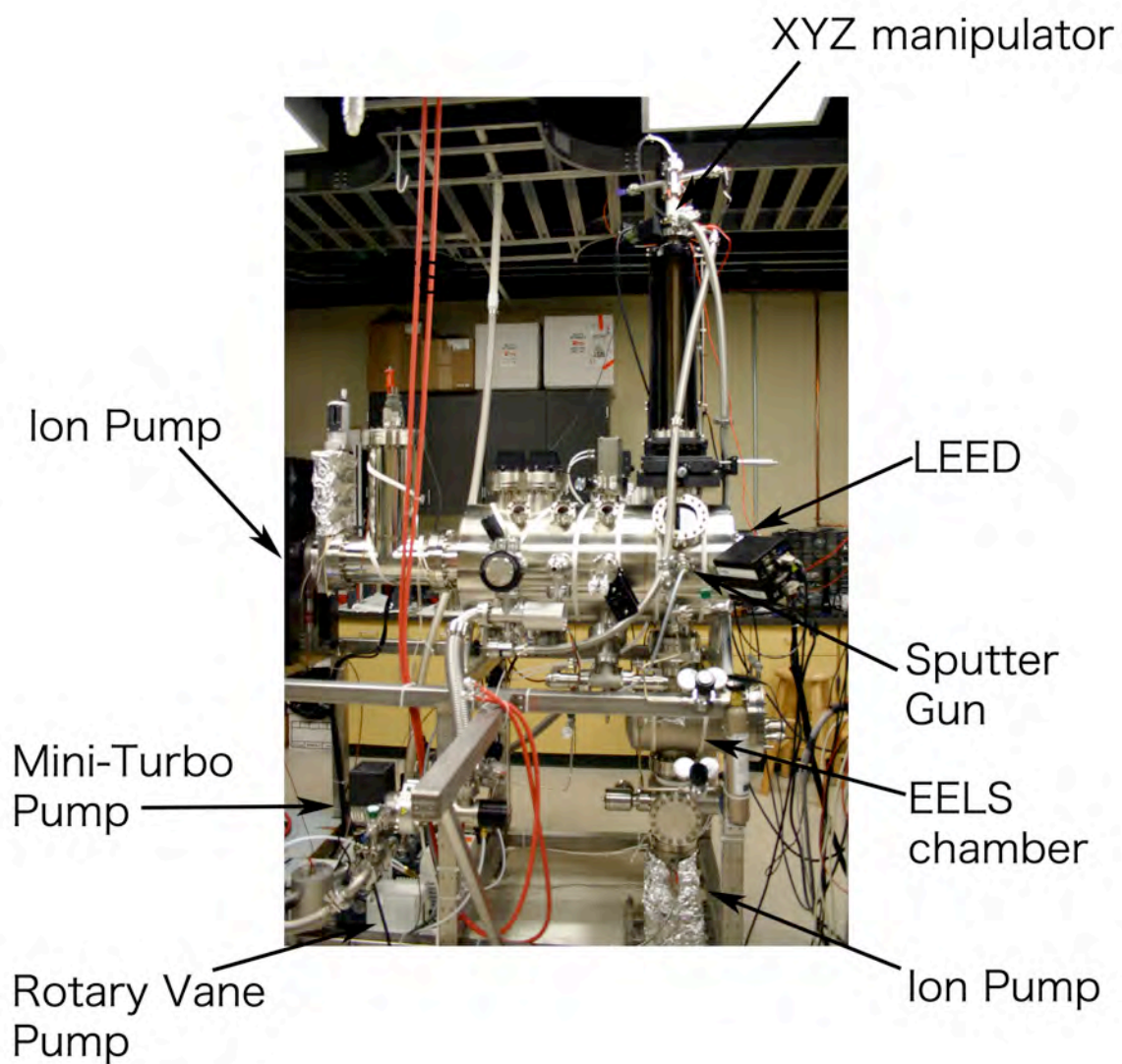


Figure 3.1. Ultra-high vacuum chamber.

A rotary vane pump is a positive displacement pump that uses a rotary motion to move gas molecules from one volume to another volume. The intake is connected to the vacuum chamber while the exhaust of the pump is exposed to atmospheric pressure. This allows for the movement of gas molecules from within the vacuum chamber to the atmosphere of the lab. This type of pump allows for pressures of 10^{-3} Torr to be reached. The vacuum limit of 10^{-3} Torr results from slight leakage around the seals of the pump

and from the use of vacuum pump oil for lubrication, which will slightly vaporize at this pressure. To prevent back-streaming of these oil vapors into the vacuum chamber, a trap made of a zeolite material is attached to the intake of the pump and is used to absorb the oil vapors.

The next phase in pumping is the turbo pump. A turbo pump is a type of momentum transfer pump, in which gas molecules are accelerated from the vacuum chamber side of the pump to the exhaust side of the pump. This is achieved with rotating blades that hit entering gas molecules and pushes them to the other end of the pump, similar to a fan. This type of pumping is used only at low vacuum pressures (the molecular flow regime) because gas molecules behave differently at different pressures. At higher pressures the gas molecules push on each other (the laminar flow regime) and are ineffectively pushed out of the vacuum chamber. This is why a primary pumping station, the rotary vane pump, is used in conjunction with the turbo pump. Typically, the exhaust pressure of the turbo pump should be maintained at 10^{-2} Torr or lower, to give optimum performance of the pump. This combined setup achieves pressures as low as 10^{-8} Torr before bakeout of the chamber. The main chamber has a turbo pump with a pumping speed of 360 L/s and the load lock has a mini-turbo pump with a pumping speed of 50 L/s.

The vacuum system also has two ion pumps, one attached to the electron energy loss spectroscopy (EELS) chamber and the other attached to the main LEED chamber. An ion pump, sometimes referred to as an ion getter pump, works by ionizing gas molecules within the pump and accelerating them across an electric potential. The accelerated

molecules collide with a titanium plate and chemically react with the titanium, trapping them within the plate itself. This effectively removes the molecules from the chamber, resulting in a virtual pumping action that can lower the pressures to 10^{-11} Torr. Since this is a capture pump, it should not be used at pressures higher than 10^{-5} Torr because the lifetime of the Ti elements will be severely shortened. The ion pump on the main chamber has a pumping speed of 500 L/s and the ion pump on the EELS chamber has a pumping speed of 60 L/s. Although ion pumps pump reactive gases very well, they do not pump inert gases such as argon very well at all. Therefore, ion pumps are usually used in conjunction with turbo pumps.

The last pump that is used on the main chamber is a titanium sublimation pump (TSP). The TSP is composed of a wire of titanium that partially evaporates when a current between 42 and 45 A is passed through it. This process is known as flashing the TSP. The evaporated titanium condenses on the inner walls of its container, coating a layer of activated titanium, which is exposed to the vacuum. Incident gas molecules react with this layer of titanium, permanently trapping it to the inside of the pump, aiding in the quality of the UHV. As with the ion pump, only reactive gases are pumped with the TSP. The TSP is the most effective pump for pumping H_2 in the chamber.

Gas molecules that adsorb to the inner surfaces of the chamber during venting to atmosphere will remain trapped for prolonged periods of time and desorb during initial pump down of the chamber. This slow desorption of the chamber's walls degrades the quality of the vacuum and prevents the pressure from reaching 10^{-10} Torr. In order to

remove the adsorbed gases from the chamber walls, the entire chamber is baked at 150 °C. This is achieved by wrapping the system with heater tapes, which are composed of metal heater wires covered in a fiberglass sheath. A current is run through the tape, heating the tape and allowing the heat to transfer to the chamber through conduction. The system is covered in thermal blankets during bakeout to prevent the external atmosphere from cooling the chamber. After baking out the entire system for at least 24 hours, the system is cooled and UHV (10^{-10} Torr) is achieved with the above pumping system.

C. SAMPLE HOLDER

Although the measurements performed in this research project were primarily LEED measurements, the system is designed such that samples can be inserted into the main chamber from the load lock, transferred to a horizontal manipulator for transfer between a scanning tunneling microscope (STM) and the LEED, and transferred from the horizontal manipulator to a vertical manipulator for EELS measurements. Since the horizontal manipulator was still in construction during the time of these measurements, the sample was mounted directly on the vertical manipulator for the LEED studies. To allow use of the vertical manipulator, a custom sample holder was designed and built that allows sample transfer and heating and cooling of the sample.

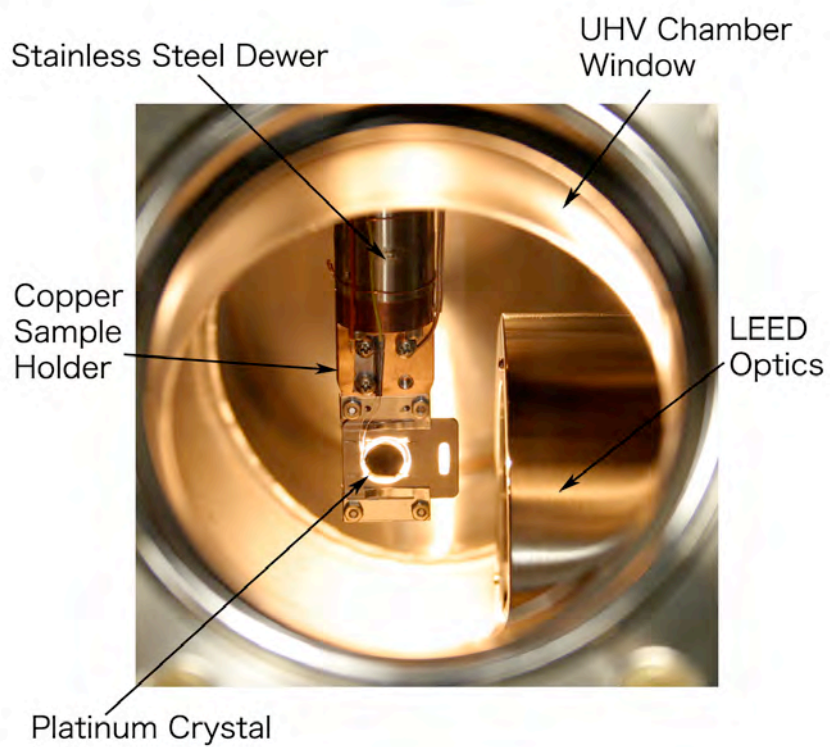


Figure 3.2. Copper sample holder in UHV.

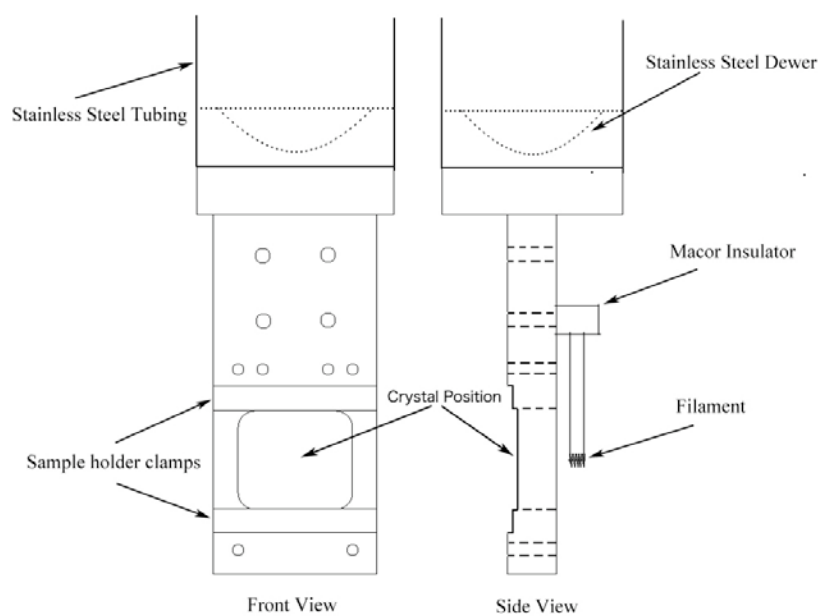


Figure 3.3. Schematic of copper sample holder.

The sample holder is made out of copper for its ability to transfer heat from or to the sample. The copper is attached to a custom stainless steel dewer using four stainless steel screws. The dewer is a hollow tube with a dimpled heat-sink welded into the bottom, where the copper holder is screwed onto it. Liquid nitrogen can be poured down the hollow tube of the dewer to cool the sample holder to temperatures below $-175\text{ }^{\circ}\text{C}$. To allow mounting of samples, the sample holder has two machined slots with molybdenum clips attached so that a rectangular sample holder plate can be attached to the copper sample holder (Fig 3.3). The sample holder plate has a $3/32'' \times 1/4''$ slot at the end to allow clamping of the sample holder with a wobble stick for transfer to the horizontal manipulator.

The sample is heated by passing a current through a tungsten filament that sits behind the sample plate (Fig 3.3). The filament is clamped to the backside of the copper sample holder with an electrically insulating ceramic called macor. Macor is chosen for its particular properties: a machinable ceramic with low thermal expansion ($93 \times 10^{-7}\text{ m/m}\cdot\text{K}$) and low thermal conductivity ($1.46\text{ W/m}\cdot\text{K}$) [8]. It is stable at high temperatures and will not outgas much in UHV. A rectangular hole was milled into the center of the copper sample holder to allow for radiation heat transfer from the filament to the sample. The top of the dewar tube is welded to a conflat flange that is mounted at the top of the vertical manipulator. A ceramic vacuum break is used to electrically isolate the dewar tube and sample holder from the grounded chamber. This design also normally allows the sample to be heated using e-beam heating by biasing the sample to extract electrons from the hot filament and accelerate them into the sample. However, it was

found after assembly of the system and baking of the chamber that the distance from the outside diameter of the dewar tube to the inside diameter of the z-bellows of the vertical manipulator was so close that an electrical discharge occurred when the sample was biased to 750 V. Therefore, we only used radiative heating of the crystal in this study.

The sample holder plates are made of 0.040" thick Mo with a dimension of 0.90" x 1.20". The plate used to mount the Pt(111) crystal has a 0.50" diameter hole bored in it. The Pt(111) crystal is mounted to the plate by first spot welding a 0.010" diameter Ta wire to top and bottom edges of the crystal followed by spot welding the wires to the Mo sample plate. Therefore, the back side of the Pt(111) crystal faces the heater filament. The temperature of the sample is monitored using a type-k thermocouple that is spot welded onto the side of the Pt(111) crystal. A thermocouple is a joining of two different materials that produce voltages that correspond to specific temperatures. The temperature of the thermocouple, and thus the sample, can be monitored by using a voltmeter to measure the voltage across the thermocouple. Using radiative heating, a crystal temperature of 700 °C can be achieved. Sample temperatures as low as -155 °C can be achieved by filling the dewar with liquid nitrogen.

The motion of the sample in UHV is achieved by using an XYZ manipulator (Fig. 3.1). The XYZ manipulator consists of two stages: a Z-stage and an XY-stage. Both stages use a stainless steel bellows to allow translation of the sample without breaking UHV. The XY-stage allows for ± 2 " travel in either the X or Y direction, and the Z-stage allows 20" of travel in the Z direction. At the top of the XYZ manipulator is a differentially pumped

rotary motion feedthru that allows for rotation of the sample over a complete 360°. This feedthru uses a series of Teflon seals, and the space between each seal is pumped on so that UHV can be maintained. The space between the first and second seals is pumped on by a rotary vane pump, and the space between the second and third seals is pumped on by the load lock turbo pump.

D. LOW ENERGY ELECTRON DIFFRACTION

Low energy electron diffraction (LEED) is a method used to determine the crystal structure of the surfaces of materials. The method takes advantage of the wave-like nature of electrons originally proposed by Louis de Broglie in 1924 when he was a graduate student. His hypothesis was that material particles also behave as waves. The wavelength of a particle with momentum p is given by $\lambda = h/p$, where h is Plank's constant. Louis de Broglie's theory was confirmed by Lester Germer and Clinton Davisson in 1927 [9]. They scattered electrons at a target of crystalline nickel and found that the angular dependence of the intensity of the scattered beam was consistent with a diffraction pattern.

In LEED, electrons are accelerated towards the sample via an electron gun. The filament of the electron gun is held at a negative potential V_{fil} with respect to ground so that electrons leave the gun with a kinetic energy eV_{fil} . By adjusting the potential of the filament, different kinetic energies of the incident electrons can be obtained. The LEED optics consists of a series of four hemispherical grids and a phosphor coated

hemispherical screen, as shown in Figure 3.4. To perform LEED measurements, the electrons from the electron gun are incident upon the crystal and reflect back towards the LEED optics. The first grid is normally held at ground potential to create a region free of electric fields. The second and third grids are held at a potential close to the potential of the filament. Therefore, these grids act as a filter to prevent inelastically scattered electrons from passing to the phosphor screen. The fourth grid is normally held at ground potential. The LEED has a screen that is coated with phosphor and is normally held at a potential between 3 kV and 5 kV so that the diffracted electrons have enough kinetic energy to excite transitions in the phosphor to emit visible light. Since the electrons behave as waves, they produce an image on the LEED screen that represents the reciprocal lattice of the crystal. The LEED screen used in our measurements is made of an indium tin oxide (ITO) coated glass hemisphere with a phosphor coating. The ITO acts as a transparent conducting surface. Because the screen is made from glass, the LEED pattern can be seen from either the front or rear of the LEED optics.

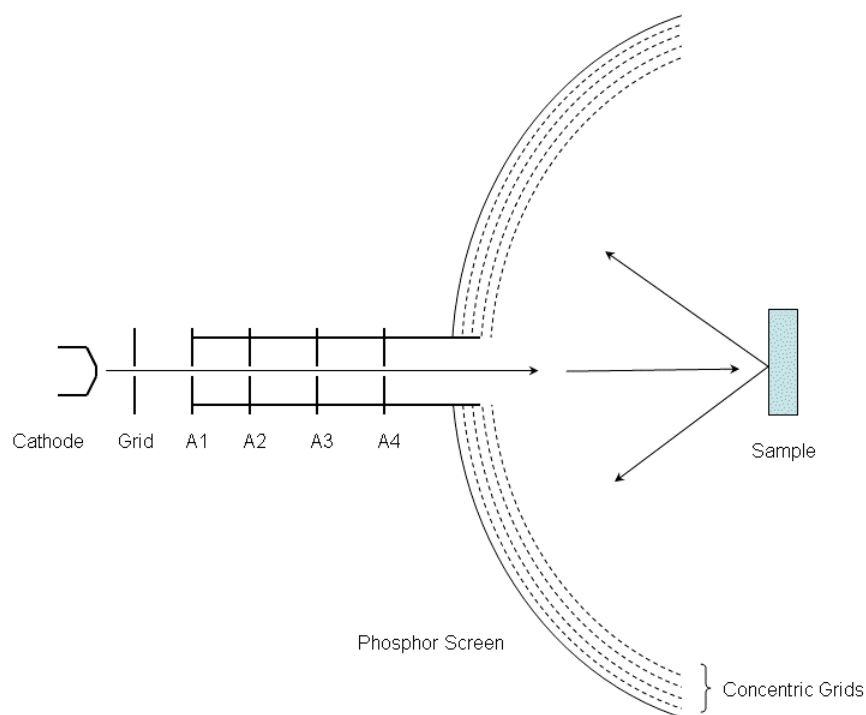


Figure 3.4. Schematic of the LEED optics [10].

Knowing the energy of the incident electron beam provides us with the de Broglie wavelength of the beam

$$\lambda = \frac{h}{\sqrt{2mE}} = \frac{12.27}{\sqrt{E}} \text{ (\AA)}, \quad [3.11]$$

where E is given in eV . By measuring the positions of the spots relative to the edge of the LEED screen for a particular electron energy, the lattice constants of the surface of the crystal can be determined. When an adsorbate has been dosed onto the surface of the material then the LEED pattern can also reveal the size and orientation of the adsorbate's

unit cell with respect to the unit cell of the underlying material.

The condition for constructive interference for a diffraction experiment is that the difference in distance from one source to another is equal to an integer multiple of the wavelength,

$$|\mathbf{r}_1| - |\mathbf{r}_2| = n\lambda . \quad [3.12]$$

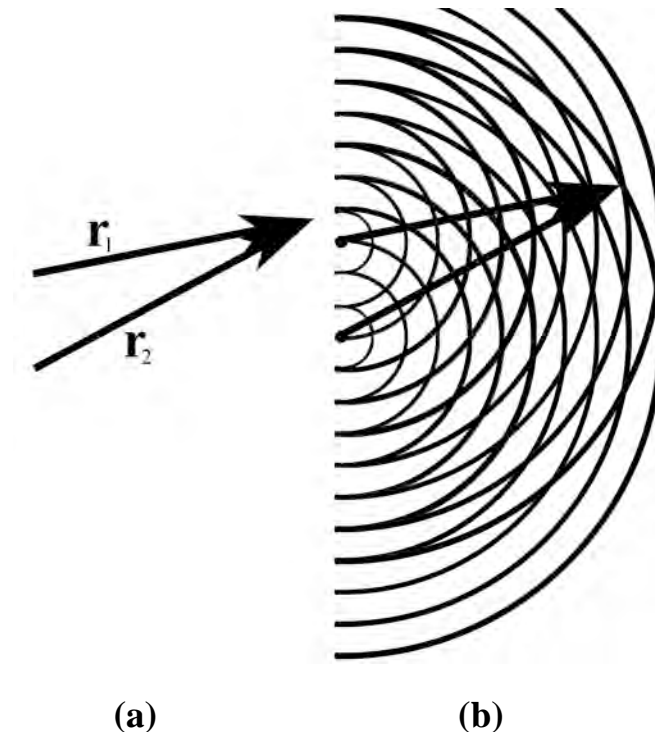


Figure 3.5. Schematic of (a) the vectors \mathbf{r}_1 and \mathbf{r}_2 from the two wave sources to a point of constructive interference and (b) the super-positioned wave crests.

It is from this constructive interference relation that we are able to view the two-dimensional reciprocal lattice of the crystal's surface. A plane wave is defined by

$$\Psi(r, t) = Ae^{i(\mathbf{k}_o \cdot \mathbf{r} - \omega t)} , \quad [3.13]$$

where \mathbf{k}_o is the wave vector and ω is the angular frequency. Then the wave function of a

scattering event with single point results in a spherical wave that can be given by

$$\Psi = f \frac{A}{D} e^{i(\mathbf{k} \cdot \mathbf{D} - \omega t)}, \quad [3.14]$$

where D is the radial distance from the scattering point and f is the scattering power; for atoms it is also known as the atomic form factor.

The atomic form factor is the scattering amplitude of the outgoing spherical wave. It can be defined as

$$f(Q) = \int_0^{\infty} \rho(r) e^{i\mathbf{Q} \cdot \mathbf{r}} dr, \quad [3.15]$$

where $\rho(r)$ is the spatial density of the scattering atom and \mathbf{Q} is the momentum transfer.

If there are two scattering events separated in space then the resulting scattering wave function can be approximated as

$$\Psi = f \frac{A}{D} e^{i\mathbf{k} \cdot \mathbf{D}} [e^{i\mathbf{s} \cdot \mathbf{r}_1} + e^{i\mathbf{s} \cdot \mathbf{r}_2}], \quad [3.16]$$

where \mathbf{r}_1 and \mathbf{r}_2 are the position vectors of the two scattering points relative to the origin.

And \mathbf{s} is the scattering vector defined as

$$\mathbf{s} = \mathbf{k} - \mathbf{k}_o. \quad [3.17]$$

Note that it is assumed that D is much larger than the distance between the points \mathbf{r}_1 and \mathbf{r}_2 and therefore the denominator of the amplitude can be approximated to D alone. This can be generalized to scattering from n -bodies by

$$\Psi = f \frac{A}{D} e^{i\mathbf{k} \cdot \mathbf{D}} \sum_n e^{i\mathbf{s} \cdot \mathbf{r}_n}. \quad [3.18]$$

A real crystal lattice is defined as

$$\mathbf{R} = l_1 \mathbf{a} + l_2 \mathbf{b} + l_3 \mathbf{c} , \quad [3.19]$$

where \mathbf{a} , \mathbf{b} and \mathbf{c} are the lattice vectors. Scattering events from this lattice result in the wave function

$$\Psi = f \frac{A}{D} e^{i\mathbf{k} \cdot \mathbf{D}} \sum_{l_1, l_2, l_3} e^{i\mathbf{s} \cdot (l_1 \mathbf{a} + l_2 \mathbf{b} + l_3 \mathbf{c})} . \quad [3.20]$$

The condition for constructive interference is that the sum must be finite which means that \mathbf{s} must simultaneously satisfy the following three conditions:

$$\mathbf{s} \cdot \mathbf{a} = h2\pi , \quad [3.21]$$

$$\mathbf{s} \cdot \mathbf{b} = k2\pi , \text{ and} \quad [3.22]$$

$$\mathbf{s} \cdot \mathbf{c} = l2\pi . \quad [3.23]$$

where h , k and l are integers [7].

Since the reciprocal lattice for this crystal is defined by

$$\mathbf{G} = n_1 \mathbf{a}^* + n_2 \mathbf{b}^* + n_3 \mathbf{c}^* , \quad [3.24]$$

and using the orthogonality condition between the reciprocal lattice vectors and the real lattice vectors the following relationship holds:

$$\mathbf{G} \cdot \mathbf{R} = n_1 \mathbf{a}^* \cdot l_1 \mathbf{a} + n_2 \mathbf{b}^* \cdot l_2 \mathbf{b} + n_3 \mathbf{c}^* \cdot l_3 \mathbf{c} . \quad [3.25]$$

Substituting the definition of each reciprocal lattice vector yields:

$$\mathbf{a}^* \cdot \mathbf{a} = \frac{2\pi}{\Omega_c} (\mathbf{b} \times \mathbf{c}) \cdot \mathbf{a} = 2\pi , \quad [3.26]$$

$$\mathbf{b}^* \cdot \mathbf{b} = \frac{2\pi}{\Omega_c} (\mathbf{c} \times \mathbf{a}) \cdot \mathbf{b} = 2\pi , \text{ and} \quad [3.27]$$

$$\mathbf{c}^* \cdot \mathbf{c} = \frac{2\pi}{\Omega_c} (\mathbf{a} \times \mathbf{b}) \cdot \mathbf{c} = 2\pi . \quad [3.28]$$

since n_1 , n_2 , n_3 , l_1 , l_2 and l_3 are integers the reciprocal lattice satisfies the condition for

constructive interference. Therefore the reciprocal lattice is the image resolved by the LEED optics.

E. ELECTRON ENERGY LOSS SPECTROSCOPY

Electron energy loss spectroscopy (EELS) is a method for determining vibrational modes of the surface of a material [11]. This provides information about the mechanical and thermal properties of the material.

EELS involves the bombardment of a surface of a material with a narrow energy band of electrons. The energies and angle of deflection is recorded for the reflected electrons. The measured scattering angle can provide information about dispersion relation for the material under question. The material composition can be determined by the measured energy differences.

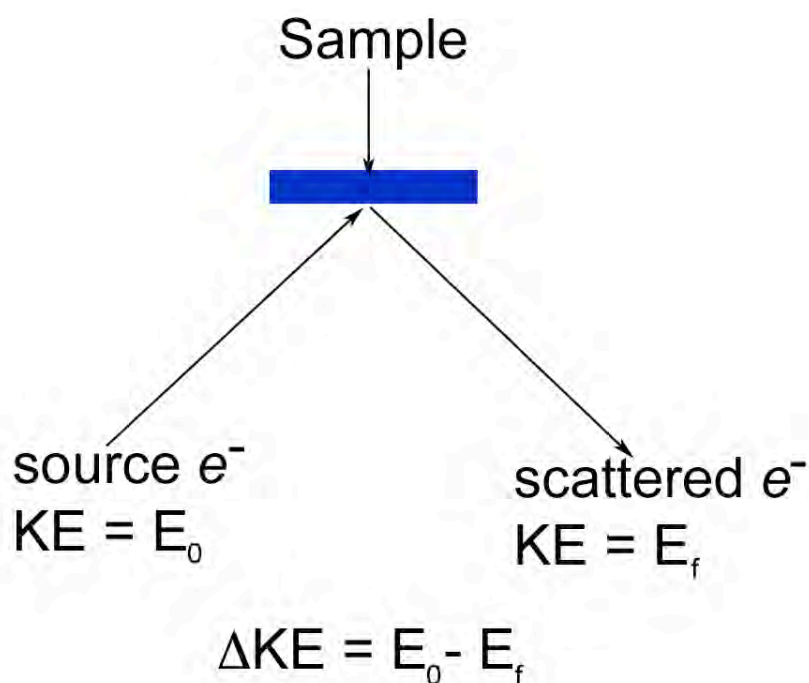


Figure 3.6. Schematic of electron energy loss spectroscopy.

EELS measurement is sensitive to external magnetic fields since magnetic fields apply a force to moving charged particles. This requires the use of a special material with a high magnetic permeability constant. Mu metal is a nickel-iron alloy that also contains copper and molybdenum. Its high magnetic permeability makes it suitable as a magnetic shield. A special chamber composed of mu metal was attached to the main vacuum chamber. The EELS instrument was installed into this chamber.

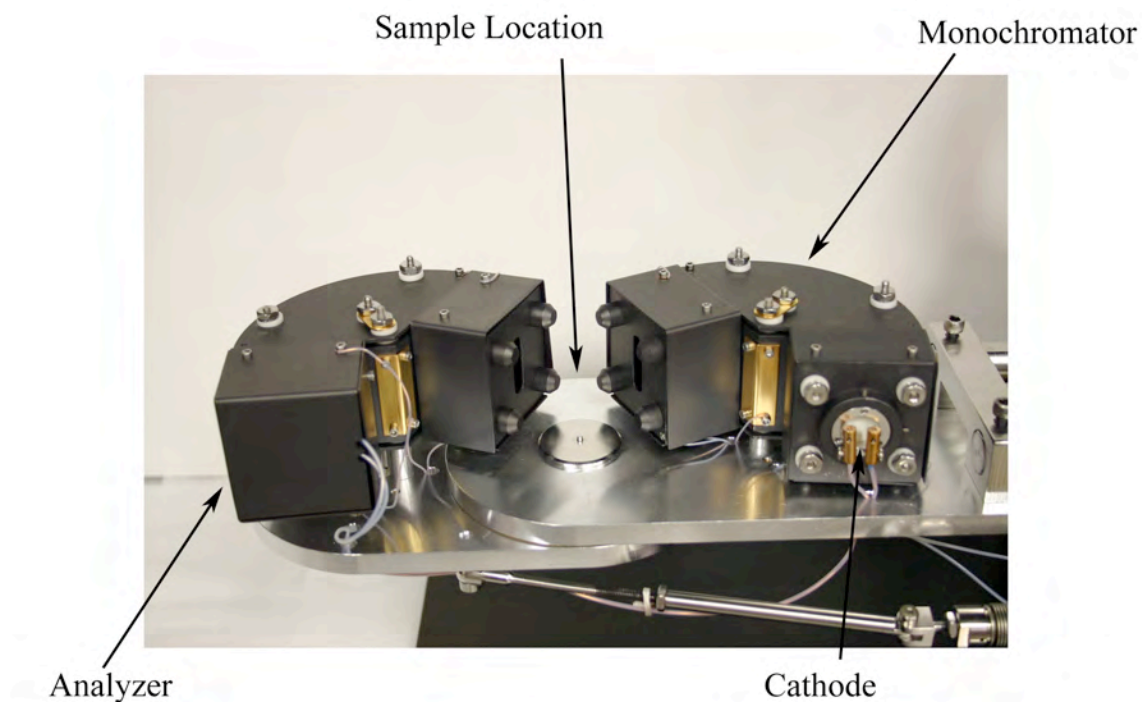


Figure 3.7. Picture of the EELS instrumentation.

The sample was transferable to the EELS electronics via the manipulation of Z-direction for the XYZ manipulator (Fig. 3.1). Once the sample was in the mu metal chamber, it could be rotated, by the use of an attached rotary manipulator, for different angles of incidence of the incoming electron beam.

Since the mu metal chamber was a smaller chamber attached to the underside of the main chamber, its vacuum would take longer to pump down. Because of this an ion pump is directly attached to the mu metal chamber. The quality of the vacuum in the EELS chamber was measured with an ion gauge attached to a pumping tee directly above the ion pump.

The EELS instrument was controlled by a digital controller connected to a computer via a serial COM port. The controller uses a software interface to interact with the user. This digital controller allows for a recording of the EELS output directly to file. This allows for a more convenient way of analyzing the collected data.

It was our intention to use the EELS chamber after every growth for a quantitative measurement of the amount of graphene produced from each recipe. However, while the software for the electronics controller of the instrument compiled and working, the controller itself did not correctly output the appropriate voltages. The output of the controller was tested by inputting each value into the software and then measuring the output with a voltmeter. Most of the voltages were correct, but some were not, while others were missing. The controller was then opened to troubleshoot the circuit, but because of the lack of the circuit diagrams, it was a much larger undertaking than there was time available for this project.

IV. EXPERIMENTAL RESULTS

A. CLEAN Pt(111) SURFACE

The substrate for graphene growth was a platinum crystal in an fcc structure that was cut along the (111) plane. Before each growth study the crystal had to be properly cleaned and ordered. The standard procedure for cleaning metal surfaces in UHV is to first sputter the surface with inert gas ions to remove the surface contaminants followed by annealing the crystal to heal the surface defects caused by sputtering.

The surface of the platinum crystal was sputtered using ionized argon atoms. The sputtering gun used a hot filament to ionize the incoming argon. The argon ions were then accelerated across a potential difference. For this research project, the energy of the ion gun was set to 1 keV with a pressure of 1×10^{-5} Torr. The sample was sputtered for 40 minutes, and the current measured off the sample was typically 12 μ A.

This process removes anything that may have adsorbed onto the surface of the surface of the platinum crystal. However, sputtering also causes disorder of the surface of the crystal. This requires that the surface be reordered by annealing the platinum crystal. To anneal the platinum, a current of 3.5 A was passed through a filament that resides a couple of millimeters behind the sample (Fig. 3.3). This heats the platinum crystal by

radiative heating. The highest temperature obtained using this method was 710 °C. The annealing process was typically maintained for 10 minutes.

Platinum single crystals are not 100% pure, they contain a certain amount of bulk carbon. For new crystals, carbon diffusion to the surface during the annealing process is a common problem. This collection of carbon on the surface will often re-crystallize upon cooling to form an atomic layer or two of graphene on the surface.

At the beginning of this study, graphene formation at the surface of the crystal was observed after sputtering and annealing even though the crystal had gone through several months of sputter-anneal cycles in previous studies. The presence of graphene on the surface is detected by the presence of a ring structure in the LEED image, as seen in Fig. 4.1a. To prepare a clean, carbon free surface for the controlled growth of graphene by decomposition of propylene, the precipitated carbon had to first be removed by exposure to oxygen at elevated temperatures. This was achieved by performing an oxygen treatment after the standard sputter-anneal process, as described below. After the anneal in UHV at 700 °C, the sample temperature was lowered by reducing the current through the filament to 2.5 A, which resulted in a crystal temperature of 500°C. At this point oxygen was dosed into the chamber through a variable leak valve to a pressure of 1×10^{-6} Torr for a total of 5 minutes. During this time the surface carbon reacts with the oxygen present in the chamber to form CO and CO₂, which desorbs from the surface. At this lower temperature, diffusion of additional carbon to the surface is suppressed. After finishing the oxygen treatment, the sample temperature was maintained at 500 °C with the oxygen leak valve closed to desorb any oxygen that might have accumulated at the

surface of the platinum crystal. After this treatment, no ring structure was observed in the LEED (Fig. 4.1b). This cleaning procedure was performed at the beginning of each day of measurements, and the surface cleanliness was checked with LEED before the controlled growth of graphene by propylene decomposition. After several months of graphene growth studies, the surface cleanliness of the platinum crystal was checked with LEED after only performing a sputter-anneal cycle, without the oxygen treatment. No ring structure was found (see Fig. 4.1c), which indicates that the amount of carbon in the bulk of the platinum was reduced to a level that is not detectable with LEED during the several sputter-anneal cycles performed in this study.

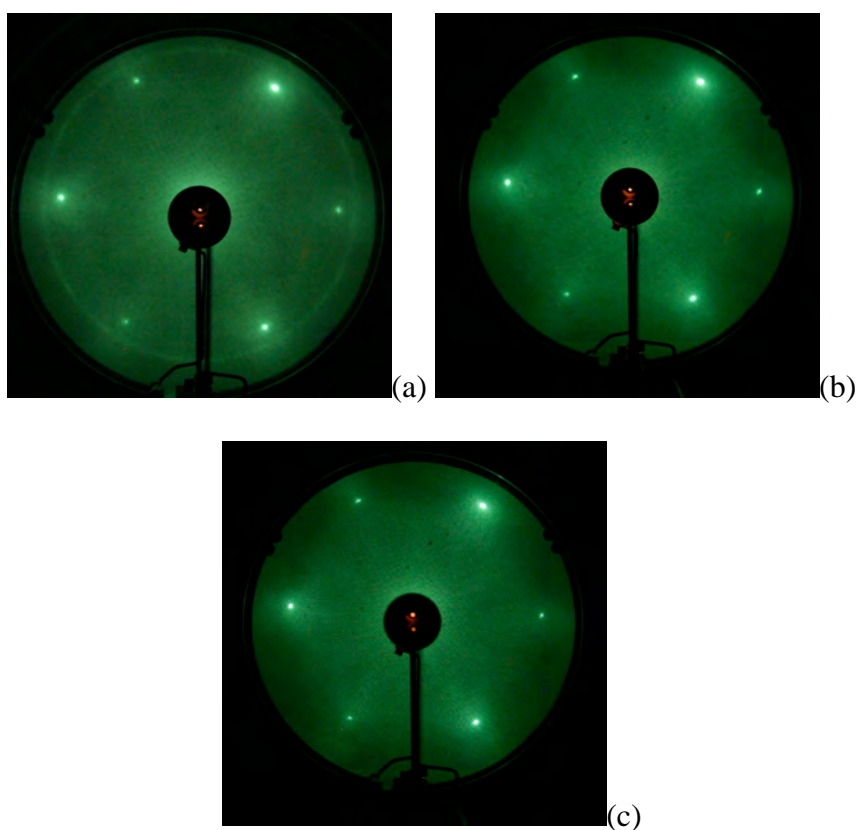


Figure 4.1. LEED of (a) high temperature anneal, no oxygen (b) post oxygen cleaning at 500 °C and (c) anneal at 500 °C, no oxygen ($E = 77.5\text{eV}$).

B. GRAPHENE GROWTH

Once we confirmed, using LEED, that the platinum crystal was clean and ordered, it was ready for the dosing procedure. In order to grow graphene on the crystal we attempted several different methods for dosing propylene.

i. Propylene deposition at room temperature followed by UHV annealing

Deposition of propylene at room temperature was first attempted. The total amount of propylene dosed on the surface is measured in units of Langmuir (L), which is defined as $1 \text{ L} = 1 \times 10^{-6} \text{ Torr}\cdot\text{s}$. The pressure in the vacuum chamber during deposition is measured using an ion gauge, and the sensitivity of the gauge depends on the gas molecule being measured. The gauge used in this study was calibrated for N_2 ; therefore, the sensitivity had to be corrected for the detection of propylene. In other words, the dose of propylene was calculated using the formula

$$D = \frac{P_{\text{gauge}} (\text{Torr}) \cdot t (\text{s})}{1 \times 10^{-6} S_r}, \quad [4.1]$$

where S_r is the relative sensitivity of the molecule being detected to that of N_2 [11]. For alkane molecules, the relative sensitivity is given by the formula

$$S_r = 1.1n + 0.4, \quad [4.2]$$

where n is the number of carbon atoms [12]. This results in a value of $S_r = 3.7$. This value was used for propylene since it is similar to the alkane molecule propane, with the exception that propylene contains a single double bond and one less hydrogen atom.

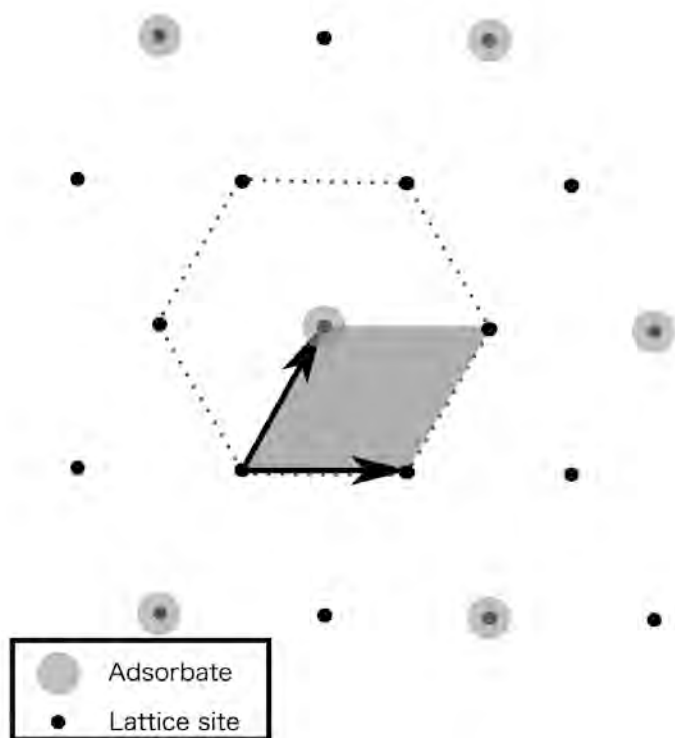


Figure 4.2. $p(2 \times 2)$ overlayer on a $fcc(111)$ lattice.

The results of room temperature deposition of propylene are shown in Fig. 4.3. After deposition of 1.6 L of propylene, a well ordered primitive 2×2 pattern was observed with LEED (Fig. 4.3b). A primitive 2×2 pattern is abbreviated as a $p(2 \times 2)$ pattern, and the corresponding structure is shown in Fig. 4.2. Since the LEED image is a picture of the reciprocal lattice, the presence of an extra spot between the Pt(111) spots indicates that the length of the basis vectors of the propylene overlayer structure is twice that of the Pt basis vectors. A similar $p(2 \times 2)$ overlayer structure was observed for a dose of 3.6 L, as shown in Fig. 4.3c, which indicates that a saturation coverage of propylene was achieved by 1.6 L.

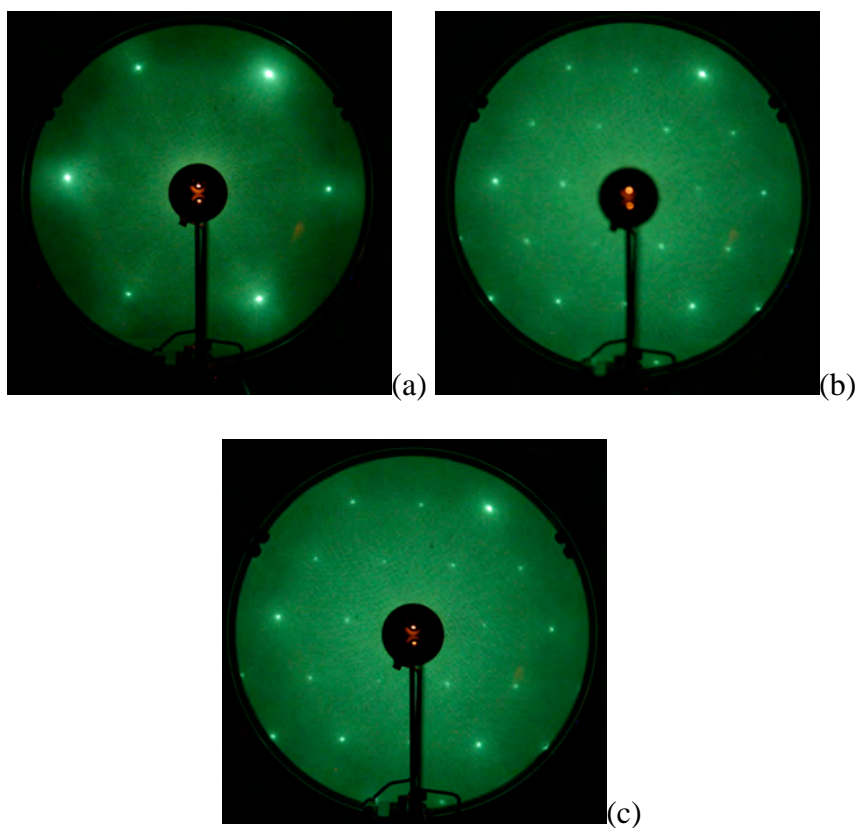


Figure 4.3. LEED of (a) clean (b) 1.6L dosing (c) 3.6L dosing at room temperature ($E = 77.5\text{eV}$).

Annealing the propylene covered Pt(111) crystal to $492\text{ }^{\circ}\text{C}$ for 10 min resulted in a loss of the $p(2\times 2)$ overlayer structure, as seen in Fig. 4.4a and 4.4b. After the 3.6L dosed sample was further anneal to $705\text{ }^{\circ}\text{C}$ for 10 min (Fig. 4.4c) the formation of a ring pattern in the LEED image was seen, which indicates the presence of a multi-domain graphene overlayer.

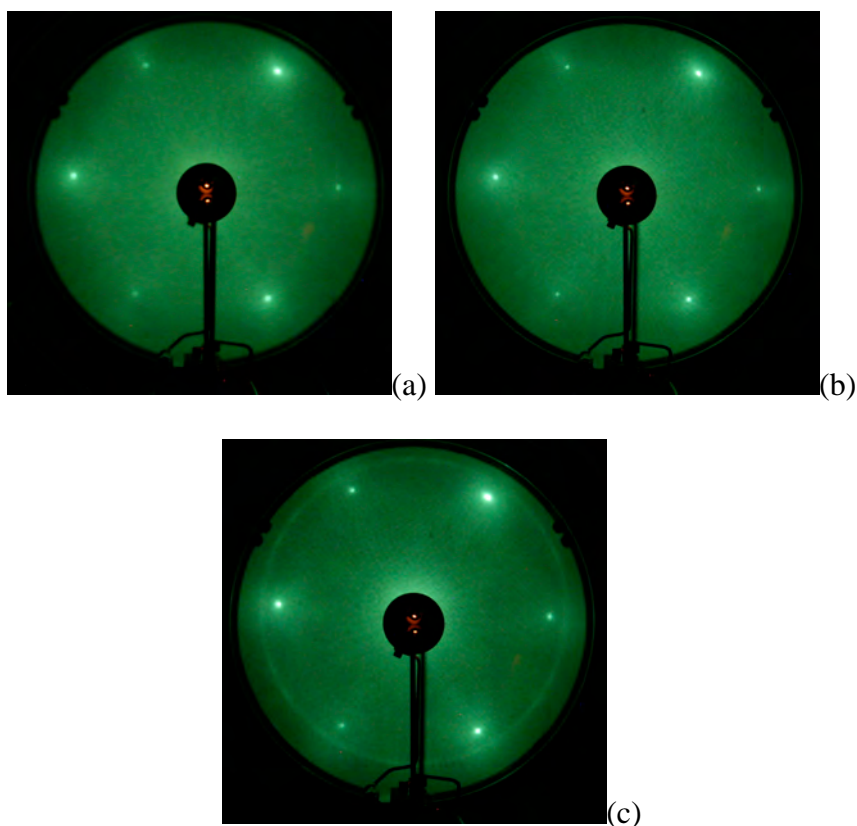


Figure 4.4. LEED of (a) 1.6L annealed at 500 °C (b) 3.6L annealed at 500 °C and (c) 3.6L annealed at 700 °C ($E = 77.5\text{eV}$).

ii. Propylene deposition at low temperature followed by UHV annealing

Another attempted method for graphene growth on platinum was to perform the dosing at low temperatures and then annealing at high temperatures. The surface of the platinum crystal was cleaned using the same method as before. Afterwards, the crystal was cooled by pouring liquid nitrogen into the dewar that is attached to the sample holder. This allowed us to get the platinum sample down to temperatures as low as 98 K (-175 °C). Once the sample reached this temperature, propylene was leaked into the chamber to dose the surface. After dosing 1.1 L, LEED was performed and no sign of a $p(2 \times 2)$ overlayer structure was observed, as shown in Fig. 4.5b. An additional 4.0 L of propylene was

dosed onto the surface, which caused almost no visible change in the LEED pattern (Fig. 4.5c). The fact that no $p(2 \times 2)$ patterns were observed in the LEED images probably indicates that the propylene does not have enough mobility to form a well-ordered overlayer structure at this temperature. The lack of a change in the diffuse background after dosing an additional 4.0 L of propylene indicates that a saturation coverage was probably achieved by a dose of 1 L.

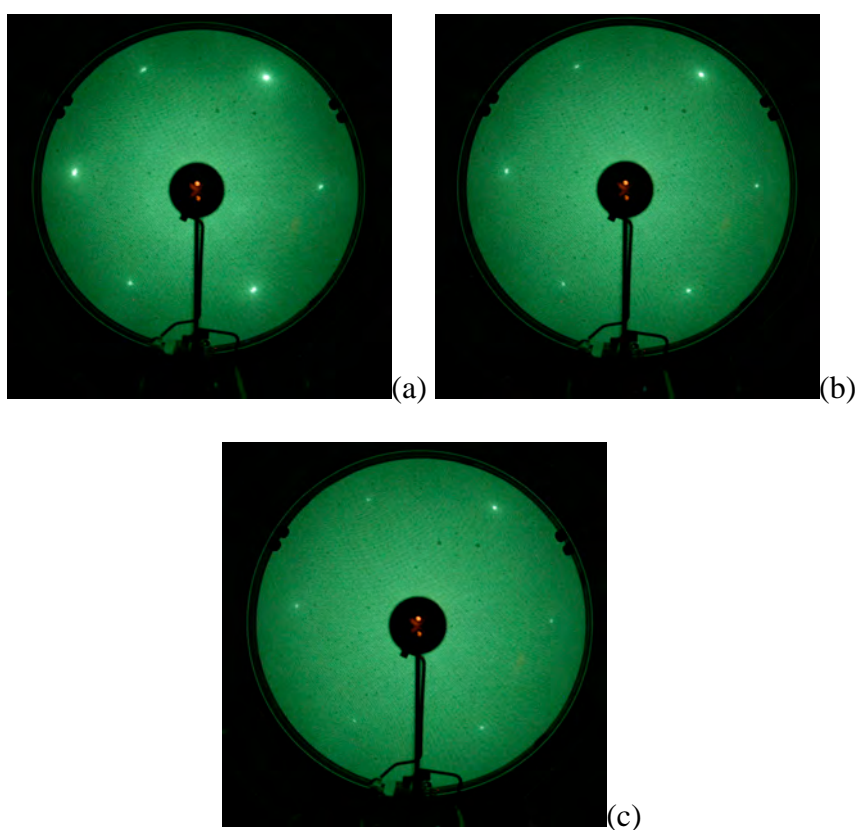


Figure 4.5. LEED of (a) clean (b) dosing 1.1L and (c) dosing 4.0L at -155°C ($E = 77.5\text{eV}$).

In order to determine the thermal stability of the propylene overlayer, the platinum crystal was annealed to 19 °C for 2 min by putting 1.5 A of current through the sample heater filament. After cooling back to -155 °C, LEED was performed but showed only the hexagonal pattern of the Pt(111) surface, as seen in Fig. 4.6a. The sample was then annealed to 710 °C for 10 min by putting 3.5 A of current through the sample heating filament. A ring structure was then observed in the LEED image (Fig. 4.6b), which indicates that a multilayer graphene film had formed on the surface.

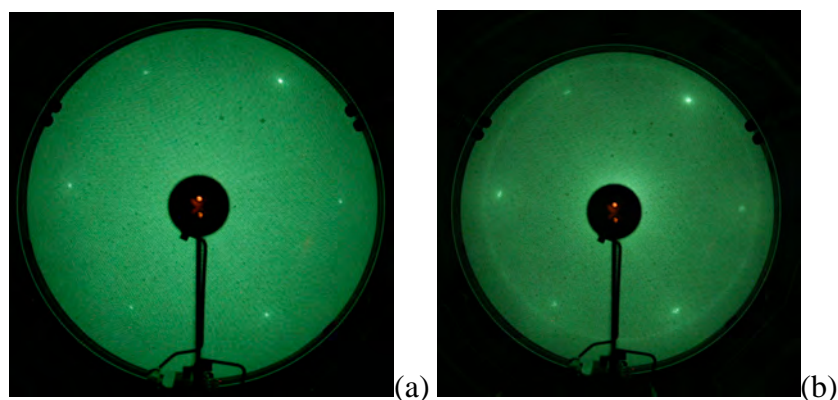


Figure 4.6. LEED after (a) anneal at room temp and (b) anneal to 700 °C ($E = 77.5\text{eV}$).

iii. Propylene deposition at high temperature followed by UHV annealing

Since carbon was not observed to diffuse to the surface of the Pt(111) crystal from the bulk at 500 °C, the grow of graphene by the catalytic decomposition of propylene was attempted at this temperature. The first preparation involved annealing the crystal at 475 °C in a propylene atmosphere of 1.5×10^{-6} Torr for 5 min, which resulted in a dose of 122 L. This preparation resulted in a large increase in the diffuse background of the LEED pattern and no ring structure associated with graphene, as seen in Fig. 4.7b. The

crystal was annealed at 703 °C for 10 min to try to order the carbon overlayer, but no ring structure or decrease in diffuse background was observed. A second anneal at 703 °C for an additional 20 min also showed no appreciable changes in the LEED pattern.

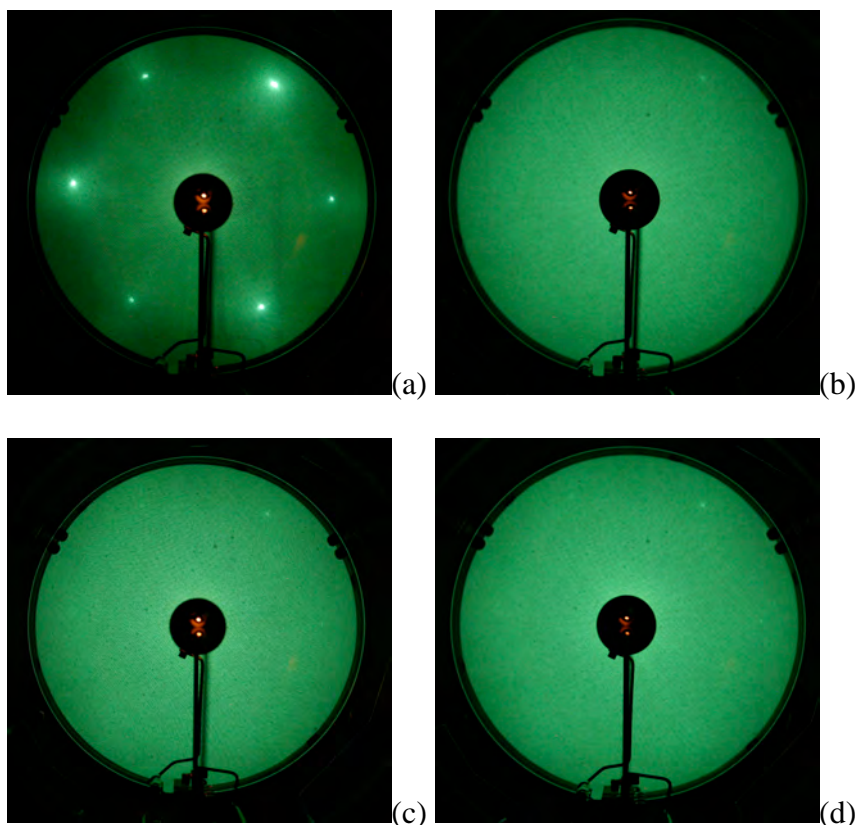


Figure 4.7. LEED of (a) clean (b) dosing 122L (c) annealed at 700 °C for 10min and (d) annealed at 700 °C for 20min ($E = 77.5\text{eV}$).

The next experiment was an anneal at 1.2×10^{-7} Torr for 5 min at a temperature of 468 °C. The LEED was unable to resolve much more than a diffuse background, implying that there was either significant coverage or the surface had disordered (Fig 4.8b). An anneal was then performed in UHV at a temperature of 708 °C for 10 minutes. Afterwards, there was still no ring observed (Fig 4.8c).

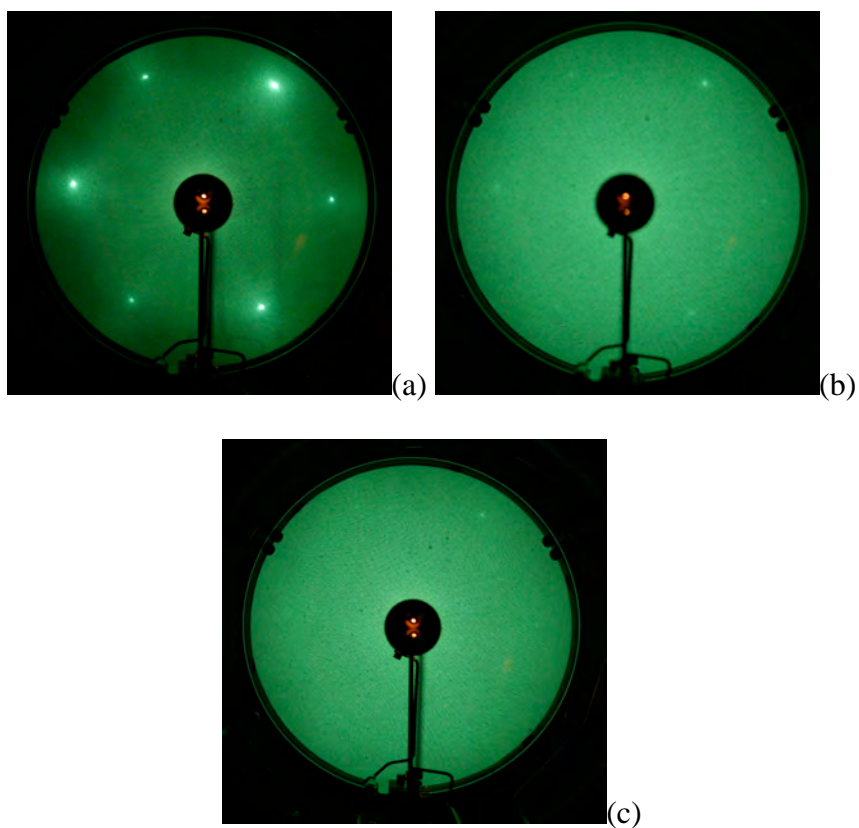


Figure 4.8. LEED of (a) clean (b) dosing 6.1L and (c) annealed at 700 °C for 10min ($E = 77.5\text{eV}$).

The final experiment was the dosing of 0.97L of propylene at a temperature of 469 °C (Fig. 4.9b). No ring structure was observed until after an anneal in UHV at 700 °C for 10 minutes (Fig. 4.9c). The crystal was then cooled, with liquid nitrogen, to a temperature of -165 °C to attempt an increase in the definition of the ring image with the LEED optics (Fig 4.9d).

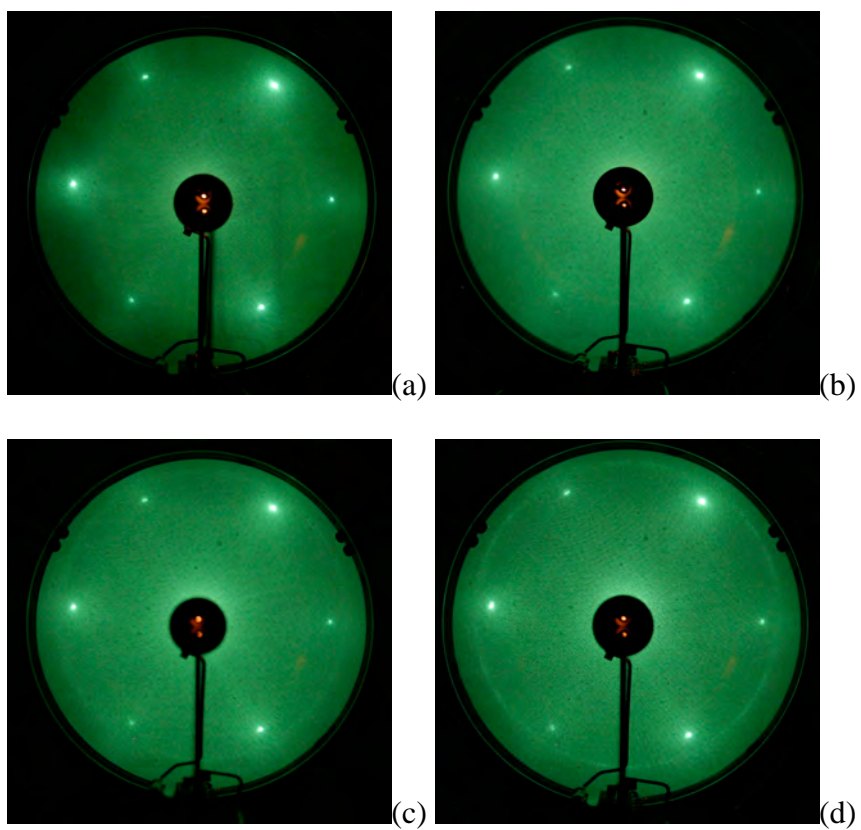


Figure 4.9. LEED of (a) clean (b) dosing 0.97L (c) annealing at 700 °C for 10min and (d) low temperature LEED at -165 °C ($E = 77.5\text{eV}$).

V. DISCUSSION

Carbon is slightly soluble in platinum. It has been measured to about 0.5% atomic carbon to atomic platinum in the temperature range of 800 °C – 900 °C as seen in Fig.

5.1. It is well known from previous studies of Pt surfaces that graphite often forms on the surface after sputtering and annealing . This is caused by carbon impurities in the bulk diffusing to the surface of the crystal during the annealing process and precipitating out as graphite during the cooling process [5]. The reason for the precipitation of carbon as it is cooled is that the carbon solubility drops as the temperature is lowered. One of the main goals of this research project was to determine if well-ordered graphene could be formed on Pt(111) at temperatures low enough to prevent solvation of carbon into the surface region.

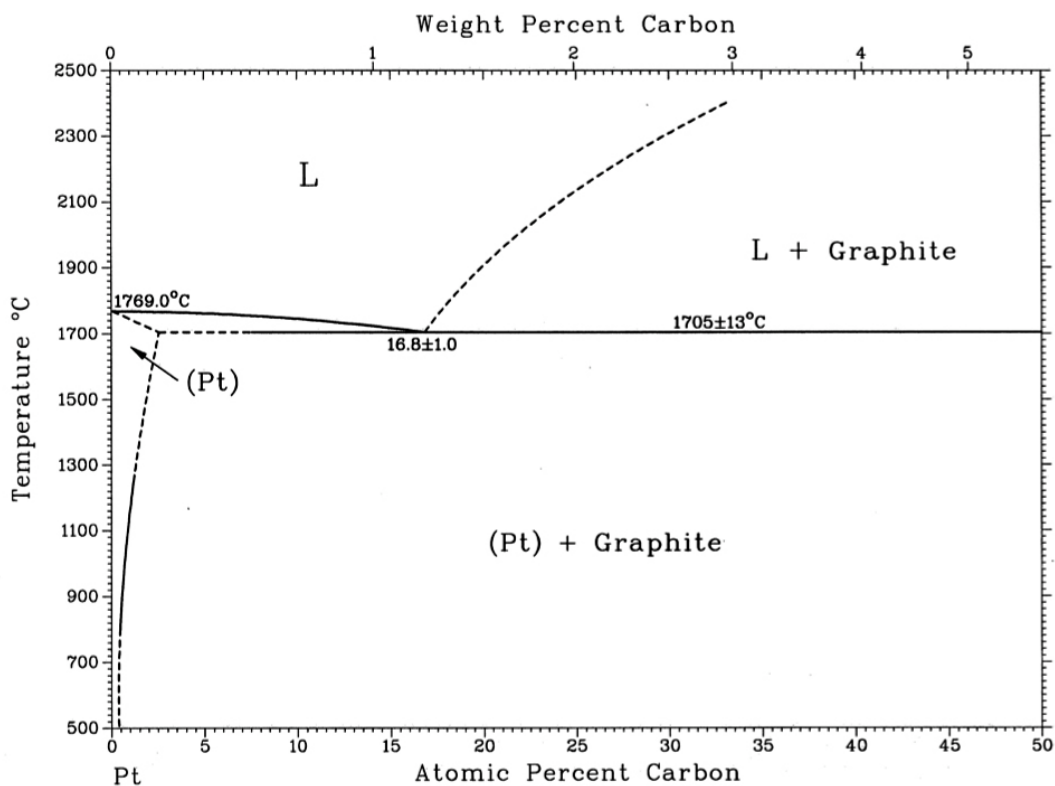


Figure 5.1: Temperature dependent platinum-carbon solubility [14].

The preparation of the Pt(111) surface by sputtering and annealing to 700 °C during the initial stages of this study resulted in the formation of a ring structure in the LEED images (see Fig. 4.1a). This provides evidence that the accumulation of carbon into the surface region from the bulk is sufficient at this temperature to cause graphite/graphene precipitation. The observation of a ring structure instead of spots indicates that the graphene overlayer formed at this temperature is non-epitaxial. In other words, the graphene is forming crystallites with a random orientation with respect to the Pt(111) surface.

To prepare a carbon-free surface, the crystal was annealed in O₂ at 500 °C to convert the carbon into CO and CO₂, followed by an anneal at 500 °C without oxygen to remove any chemisorbed oxygen from the surface. Since a LEED pattern with no ring structures and very low diffuse background were observed after the 500 °C anneal without O₂, the mobility of carbon in Pt at this temperature must be low enough to prevent carbon diffusion to the surface region. This is the reason why our attempts to grow an epitaxial graphene layer by catalytic decomposition of hydrocarbon molecules were performed at temperatures no higher than 500°C. To allow a low decomposition temperature, we chose the hydrocarbon source propylene, which has a carbon-carbon double bond.

The deposition of propylene at room temperature formed a well-ordered chemisorbed layer, as determined by the formation of a sharp p(2x2) LEED pattern (Fig 4.3b). Annealing to 500 °C resulted in the loss of the p(2x2) pattern with no formation of a ring structure. This indicates that the propylene had decomposed into carbon by that temperature but had not crystallized into graphene. Only after annealing to 700 °C was a ring structure observed. This was also true for the deposition of 1 L of propylene at 500 °C, where only an increase in diffuse background was observed at the growth temperature. A ring pattern was observed after a post-anneal to 700 °C. These results provide strong evidence that the carbon-Pt interaction is not strong enough to order the carbon atoms into graphene at 500 °C. On the other hand, previous studies of the deposition of either ethylene or propylene on the Ni(111) surface at 500 °C found that an epitaxial graphene layer could be formed [15-16]. This shows that the carbon-Ni interaction must be much stronger than the carbon-Pt interaction.

Using LEED alone, it is not possible to determine the decomposition of the propylene. It may be possible that the propylene disorders on the surface, breaks down into other hydrocarbons or it may even completely desorb from the surface of the crystal. The use of EELS is necessary to determine what is left on the surface of the platinum. However, the EELS controller was not working properly. Therefore, it will be necessary to either replace or rebuild the controller before an EELS measurement can be made.

The observation that the diffuse background of the LEED images continued to rise as the propylene dose at 500°C was increased, indicates that some of the carbon formed during the dissociation process must be dissolving into the Pt surface region. Otherwise, one would expect that the dissociation process would stop after about a monolayer of carbon had formed since this process needs catalytically active Pt atoms available.

It may turn out that even higher temperatures are required to effectively produce graphene. In a previous LEED study of this same crystal [17], it was found that annealing the Pt crystal to 1000 °C resulted in a quasi-epitaxial graphite overlayer since both a ring structure and spots corresponding to multi-domain graphite structure were observed, as shown in Fig. 5.2. In order to perform these higher temperature measurements, the sample holder will need to be modified in order to allow e-beam heating. This will allow temperatures above 1000 °C to be reached. In addition, it will be necessary to use STM to determine if the crystalline carbon growth is growing uniform sheets of graphene, or if there are islands of graphite that form.

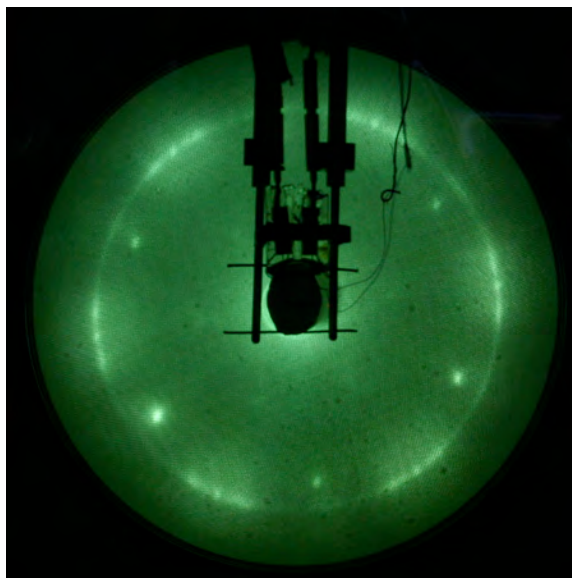


Figure 5.2: LEED result of the Pt(111) crystal annealed to 1000 °C ($E = 77.5$ eV) [17].

VI. CONCLUSIONS

Platinum had been chosen as the substrate to study the growth of graphene for two main purposes. The surface of the platinum (111) crystal has a close-packed arrangement of atoms, which has the same hexagonal symmetry as the two-dimensional graphene crystal, and platinum is a natural catalyst of hydrocarbons, which causes hydrocarbon molecules to dissociate upon contact.

It was hoped that the dosing of propylene onto platinum (111) would allow for the cracking of propylene into decomposed forms of hydrocarbons that would then adsorb to the surface. The purpose for using a catalytic substrate is to allow for the growth of graphene at relatively low temperatures (below 700 °C) since higher temperatures wouldn't be required to dissociate the propylene into its constituent components. This would also allow for single layer graphene to grow since once all the platinum sites are covered, there should not be any more sites available for additional propylene molecules to catalytically decompose. With the temperature too low to thermally decompose the propylene molecule, only a single layer of graphene would be able to form.

It is apparent from the LEED patterns that graphene formation did not occur at temperatures of 500 °C. Graphene formation was seen to begin at temperatures closer to 700 °C. However, the graphene that formed at that temperature may have come from

both the dosing of propylene and the diffusion of carbon from the bulk since it was shown that clean platinum can also form graphene at temperatures above 700 °C without any dosing.

Several recipes for graphene growth were attempted. Each recipe failed to produce graphene at temperatures of 500 °C, only at temperatures of 700 °C was graphene evident. In conclusion, it appears that the Pt(111) surface is not a good candidate for the low temperature growth of graphene.

REFERENCES

- [1] A. K. Geim and K. S. Novoselov, *Nature Mater.* **6**, 183 (2007).
- [2] K. Nomura and A. H. MacDonald, *Phys. Rev. Lett.* **98**, 076602 (2007).
- [3] K. S. Novoselov, A. K. Geim, S. V. Morozov, D. Jiang, S. V. Dubonos, I. V. Grigieva, and A. A. Firsov, *Science* **306**, 666 (2004).
- [4] W. A. de Heer, C. Berger, X. Wu, P. N. First, E. H. Conrad, X. Li, T. Li, M. Sprinkle, J. Hass, M. L. Sadowski, M. Potemski, and G. Martinez, *Solid State Commun.* **143**, 92 (2007).
- [5] J. Winterlin and M.-L. Bocquet, *Surf. Sci.* **603**, 1841 (2009).
- [6] X. Li, W. Cai, J. A., S. K., J. Nah, D. Yang, R. Piner, A. Velamakanni, I. Jung, E. Tutuc, S. K. Banerjee, L. Colombo, and R. S. Ruoff, *Science* **324**, 1312 (2009).
- [7] M. A. Omar, *Elementary Solid State Physics* (Reading, Addison-Wesley, 1975).
- [8] <http://www.corning.com/>.
- [9] C. Davisson and L. H. Germer, *Nature* **119**, 558 (1927).
- [10] <http://www.wikimedia.org/>.
- [11] G. Ertl and J. Küppers, *Low Energy Electrons and Surface Chemistry* (Weinheim, VCH, 1985).
- [12] F. Schreiber, *Progress in Surface Science* **65**, 151 (2000).
- [13] H. Si-Pu, D. F. Ogletree, M. A. Van Hove, and G. A. Somorjai, *Surf. Sci.* **180**, 433 (1987).
- [14] *C-Pt Solubility Diagram* (Materials Park, ASM International, 1996).
- [15] Y. Gamo, A. Nagashima, M. Wakabayachi, M. Terai, and C. Oshima, *Surf. Sci.* **374**, 61 (1997).

- [16] D. Y. Usachov, A. M. Dobrotvorskii, A. M. Shikin, V. K. Adamchuk, A. Y. Varykhalov, O. Rader, and W. Gudat, *B. Russ. Acad. Sci. Ph.* **73**, 679 (2009).
- [17] T. M. Sweeney, M.S. Thesis, University of New Orleans (2004).

VITA

Gregory Scott Hodges is the youngest son of McCloud and Demaris Hodges. He was born in Baltimore, Maryland on August 17, 1981, and was raised outside the city in the suburb of Parkville.

Gregory attended the schools of Baltimore County School District before graduating in May 1999. In August 1999, Gregory enrolled at Texas A&M University. At Texas A&M he studied the fields of physics and mathematics until he was awarded a Bachelor of Science in May 2005.

The following September, Gregory enrolled at the Geos Kudan Institute of Japanese Language & Culture, Tokyo, Japan to study Japanese. He returned to the United States in 2006, where he began working as a software engineer in Austin, TX.

In January 2008, Gregory enrolled at Texas State University-San Marcos to pursue his master's degree in applied physics. He began his graduate research in May 2008, emphasizing on the growth and low energy electron diffraction spectroscopy of graphene on Pt(111). He expects to graduate as Master of Physics in May 2010.

Gregory is currently working as a software engineer for id Software, Dallas, TX.

Permanent Address: 2507 Ebony Rd.

Baltimore, Maryland 21234

This thesis was typed by Gregory S. Hodges.